A STREAMBED-PARTICLE MODEL-STUDY FACILITY USING HYDROXYETHYLCELLULOSE SOLUTIONS AS A FLUID

ARS-S-147
September 1976

AGRICULTURAL RESEARCH SERVICE • U.S. DEPARTMENT OF AGRICULTURE

CONTENTS

ILLUSTRATIONS

TABLE

A STREAMBED-PARTICLE MODEL-STUDY FACILITY USING HYDROXYETHYLCELLULOSE SOLUTIONS AS A FLUID

By Neil L. Coleman and Wilbert M. Ellis[1]

ABSTRACT

Variable-viscosity long-chain polymer solutions will be used to provide a wide range of Reynolds numbers in a new facility for experimenting with the hydrodynamic forces exerted on streambed particles. Hydroxyethylcellulose solutions tested in the facility proved to have a desirable, nearly Newtonian behavior and sufficient viscosity stability. The facility can provide the needed range of Reynolds numbers, while maintaining flow-velocity profiles typical of streambed conditions. **KEYWORDS: hydraulics, hydraulic laboratories, hydraulic modeling, sediment, sediment transport, soil erosion.**

INTRODUCTION

The mechanics of the beginning of streambed-particle motion are important in problems of stable channel and riprap designs. Many experimental studies have been made to investigate the action of flow-induced forces on a streambed particle. In general, where the particle is far from the water surface, the action of streamflow upon an alluvial particle is a Reynolds-similitude phenomenon. For this reason, experiments have been made using scaled-up Reynolds models of a streambed particle. In these simulations the character of the local flow and the application of forces to the particle can be observed in a detail not possible in flume experiments.

In model studies of particles in the silt, sand, or gravel size ranges, obtainment of dynamic similitude requires operation of the model at low-particle Reynolds numbers. Since the model particle itself is large, even though the prototype is small, and since the velocities, forces, and so forth in the model must be large enough to be measured conveniently, low Reynolds numbers must be obtained by means of working fluids of a high viscosity. Furthermore, since a wide range of Reynolds numbers is generally required in the model, it is advantageous to be able to vary selectively the viscosity of the working fluid. Early work with a large-scale particle Reynolds model indicated that such conditions might be accomplished with aqueous solutions of a long-chain polymer as a working fluid, if a polymer with-sufficiently Newtonian viscosity characteristics could be found (*3*.)[2]

Many long-chain polymers are cellulose compounds, several of which are used industrially as thickeners, sizers, and adhesives. They are commercially produced in a variety of types. Depending on type, they can be dissolved in water to produce non-Newtonian fluids with drag-reducing properties or nearly Newtonian fluids that have almost stable viscosities over a wide range of shear rates.

Because of their importance in naval engineering and other applications, the drag-reducing polymer solutions have been intensively studied for nearly 30 years (*6*). Perhaps be-

[1] Geologist and hydraulic engineering technician, USDA Sedimentation Laboratory, Agricultural Research Service, Oxford, Miss. 38655.

[2] Italic numbers in parentheses refer to items in "Literature Cited" at the end of this publication.

cause of the emphasis that has been placed on drag reduction, polymer solutions with nearly Newtonian characteristics have not been used as working fluids in model studies where a wide range of Reynolds numbers is desired.

This paper describes a streambed-particle Reynolds-model facility designed to operate with Newtonian polymer solutions to study lift and drag forces on streambed particles, flow configuration and pressure distribution around particles, and the beginning of particle motion. We describe the construction and instrumentation of the facility, and the range of experimental flow conditions attainable by using a nearly Newtonian polymer solution.

THE MODEL FACILITY

Figure 1 is a schematic of the particle model-study facility that has been built, a tunnel that recirculates water. It consists of (a) a rectangular upper conduit within the working section of the model, (b) a polymer mixing box, (c) a return pipe, and (d) a propeller pump driven by a variable-speed device by a 5-hp motor. The maximum discharge of the pump is 1,100 gal/min.

The water tunnel has an auxiliary pump and gravity return system (e) for removing fluid and storing it in a holding tank (f). This system permits temporary drainage to allow access, through appropriate hatches, to the working section without wasting the polymer solution. For changing polymer solutions, there is an external drain (g). The polymer mixing box has a removable lid fitted with an air-vent valve (h) and a water-filling valve (i) with a hose fitting. A small bleed valve (j) in the upper conduit upstream of the working section allows withdrawing fluid samples to determine viscosity and density.

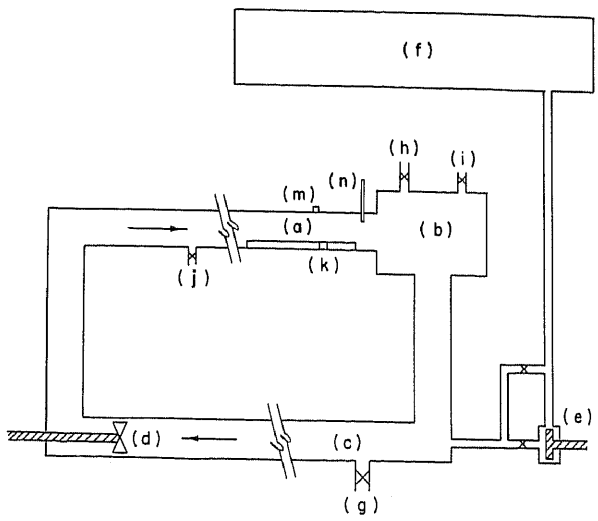

FIGURE 1.—Schematic of the model facility: (a) rectangular conduit, (b) polymer mixing box, (c) return pipe, (d) propeller pump, (e) auxiliary pump, (f) holding tank, (g) drain, (h) air-vent valve, (i) water-filling valve, (j) bleed valve, (k) circular opening, (m) packing gland, (n) thermometer.

To use polymer solutions economically in the model facility, an initial solution of a relatively high viscosity must be mixed and a complete series of experiments performed with this fluid. Then, a new fluid with a low viscosity is pro-

TABLE 1.—*Properties of HEC solutions at 77° F*

Concentration of HEC (%)	Density (slugs/ft³)	Shear rate[1] (s^{-1})	Kinematic viscosity[1,2] (ft^2/s)
0.2	1.934	1.38×10^{1}	2.08×10^{-5}
		3.44×10^{1}	2.06×10^{-5}
		6.88×10^{1}	2.02×10^{-5}
		1.66×10^{5}	1.53×10^{-5}
.4	1.934	6.88×10^{0}	4.56×10^{-5}
		1.38×10^{1}	4.35×10^{-5}
		3.42×10^{1}	4.06×10^{-5}
		6.88×10^{1}	4.19×10^{-5}
		8.00×10^{1}	3.18×10^{-5}
.6	1.934	3.44×10^{0}	1.16×10^{-4}
		6.88×10^{0}	1.13×10^{-4}
		1.38×10^{1}	1.10×10^{-4}
		3.44×10^{1}	1.04×10^{-4}
		3.54×10^{5}	7.20×10^{-5}
.8	1.934	6.90×10^{-1}	2.43×10^{-4}
		1.72×10^{0}	2.22×10^{-4}
		3.44×10^{0}	1.98×10^{-4}
		6.88×10^{0}	1.94×10^{-4}
		1.38×10^{1}	1.95×10^{-4}
		1.96×10^{4}	1.30×10^{-4}
1.0	1.934	6.90×10^{-1}	3.90×10^{-4}
		1.72×10^{0}	3.79×10^{-4}
		3.44×10^{0}	3.49×10^{-4}
		6.88×10^{0}	3.46×10^{-4}
		1.38×10^{1}	3.48×10^{-4}
		1.09×10^{4}	2.34×10^{-4}
2.0	1.953	3.40×10^{-1}	2.99×10^{-3}
		6.90×10^{-1}	3.08×10^{-3}
		1.72×10^{0}	3.12×10^{-3}
		1.61×10^{3}	2.18×10^{-3}

[1] Last value in each set of measurements was determined with a falling-ball viscosimeter, other values with a rotating-spindle viscosimeter.

[2] Each value is the average of 3 determinations made at the same shear rate.

duced by controlled dilution of the original fluid, followed by another series of experiments. The process can be repeated several times, so that an extremely wide range of experimental viscosities can be obtained with a relatively small amount of polymer.

The upper rectangular conduit (31 ft long, 0.916 ft wide, and 0.583 ft high) of the model facility is constructed of transparent plastic. The working section (a) is a bed of ½-in-diameter plastic spheres glued in a close-packed configuration to the floor of the conduit, simulating in scaled-up form a small streambed segment. The leading edge of the bed of spheres is 22.5 ft from the upstream end of the conduit. The bed is 4.6 ft long. At a point on the centerline of the bed, and 3.4 ft below the leading edge, a 3-in-diameter circular opening (k) in the conduit floor allows for the installation of equipment for measuring forces on a bed particle. A packing gland (m) in the top of the conduit, 3.35 ft from the leading edge of the bed, allows a total-head tube to be inserted for determining the velocity distribution over the bed. For monitoring hydrostatic pressure, two piezometer taps (not shown) are installed in the sidewall of the conduit near the openings (k) and (m). A thermometer (n) has been installed through the top of the conduit, just below the trailing edge of the bed to allow fluid temperature to be observed during an experiment.

PROPERTIES OF POLYMER SOLUTIONS

The polymer compound selected for use is hydroxyethylcellulose (HEC), which is commercially available. According to the manufacturer, the compound is nearly Newtonian over a wide range of shear rates and relatively unsusceptible to viscosity degradation by stirring or pumping, and it can be completely dispersed in water by stirring before it begins to dissolve. Such characteristics insure formulation of an homogeneous solution, without residual clumps of partially dissolved polymer.

Small samples of HEC solutions at various concentrations were analyzed for differences in density and viscosity (under varying shear rates), to determine the extent to which these solutions might exhibit non-Newtonian behavior. These analyses were carried out at a standard temperature of 77° F (25° C). The results are given in table 1. Each viscosity value is the average of three determinations made at the same shear rate.

The solution densities (table 1) were found by weighing measured volumes of the different solutions. The table shows that the densities of HEC solutions at 77° F do not differ appreciably from the density of water until a 2% concentration is reached. The kinematic viscosities in the table were measured with a commercial rotating-spindle viscosimeter capable of exerting eight different shear rates on a sample, and also with a commercial falling-ball viscosimeter. In the rotating-spindle viscosimeter, a cylindrical spindle with radius r is inserted into a small sample container, so that the fluid is confined to a restricted annular space with radius Δr, small relative to r. The shear rate (η) for the instrument can then be approximated as a function of spindle speed (ω) as

$$\eta = \frac{dU_t}{dr} = \frac{r}{\Delta r}\omega, \qquad (1)$$

where U_t is the tangential velocity.

With the falling-ball viscosimeter, the ball falls along the centerline of a tube, so that the fluid sample is forced through a small annulus at the diameter of the ball. The maximum shear rate (η) in the annulus is at the ball surface and can be approximated from considerations of the velocity distribution along any radius of the annulus, and shown as a function of the ball Reynolds number,

$$\eta = 180{,}000\left(\frac{2R_b W}{\nu}\right)^{1/4}, \qquad (2)$$

where R_b is the ball radius, W the ball velocity, and ν the kinematic viscosity of the fluid. Apparently (table 1), the falling-ball viscosimeter exerts substantially higher shear rates than does the rotating-spindle viscosimeter.

The non-Newtonian behavior of the HEC solutions is not pronounced: kinematic viscosity for the six solutions in table 1 decreased about 34% over an average 100% increase in shear rate. The variation of kinematic viscosity with

shear rate for these polymer solutions can be represented by

$$\frac{\nu}{\nu_1} = \left(\frac{\eta}{\eta_1}\right)^N, \qquad (3)$$

where ν_1 is the kinematic viscosity at the unit shear rate, η_1. For a perfectly Newtonian fluid, the exponent N would have the value zero. For the polymer solutions, N varies with concentration, as shown in figure 2. The relative-viscosity function expressed by equation 3 is depicted in figure 3.

Evidently, there are two ways of representing the apparent viscosity of a polymer solution used as a working fluid in the model facility. The first is to use the unit shear rate (η_1) for a particular solution, at a particular fluid temperature. However, this is not realistic with regard to actual shear rates expected in the model. The second method is to use the nearly constant (quasi-Newtonian) viscosity exhibited by the polymer solutions at high shear rates. We adopted this method to study the flow conditions in the model facility, since the high shear-rate viscosity of a given working fluid can be easily obtained with the falling-ball viscosimeter.

PERFORMANCE OF THE FACILITY

We tested the series of HEC solutions for which temperature-viscosity functions are given in figure 4, to verify that the polymer solutions would maintain constant viscosity duri pumping and to define the velocity distributio and the range of experimental conditions th could be generated in the facility.

The viscous stability of the HEC solutio was verified by comparing the temperatu viscosity function immediately after mixi and after several hours of experimental pum ing. Figure 5 shows the comparison for a 0.3 HEC solution.

Because of the wide range of viscosity of t HEC solutions, the flows generated in t facility can be expected to display time-mea velocity distributions ranging from the par bolic distribution of a completely viscous flo to the logarithmic profile of a turbulent, rou conduit flow. These velocity distributions ca all be accommodated (7) on a single grap plotted in the coordinates

$$\frac{U}{U_*} + \frac{\Delta U}{U_*} = f\left(\frac{U_* y}{\nu}\right) + \frac{\Pi}{\kappa}\omega\left(\frac{y}{\delta}\right), \qquad (4$$

where U is the time-mean velocity, y the di tance from the velocity measurement to th virtual origin of the profile, U_* the shear ve locity at the virtual origin, κ the Karman cor stant, and δ the boundary-layer thickness, take as the distance from the point where the max mum velocity U_m occurs in the conduit to th virtual origin. The ratio $\Delta U/U_*$ is the velocit

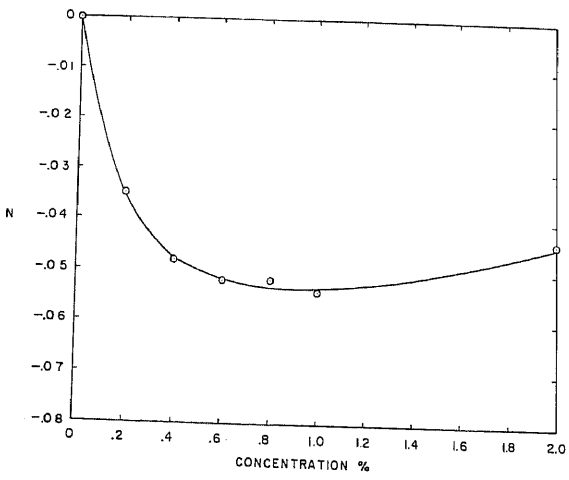

FIGURE 2.—Variation of the exponent N with polymer solution concentration.

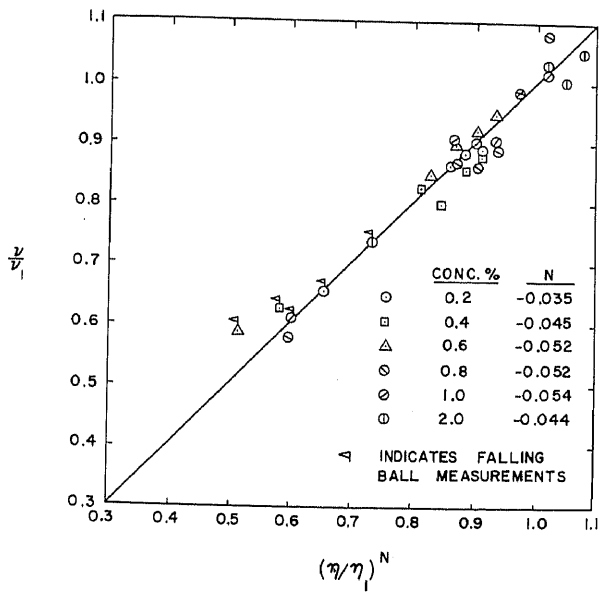

FIGURE 3.—Relative-viscosity function for HEC solu tions.

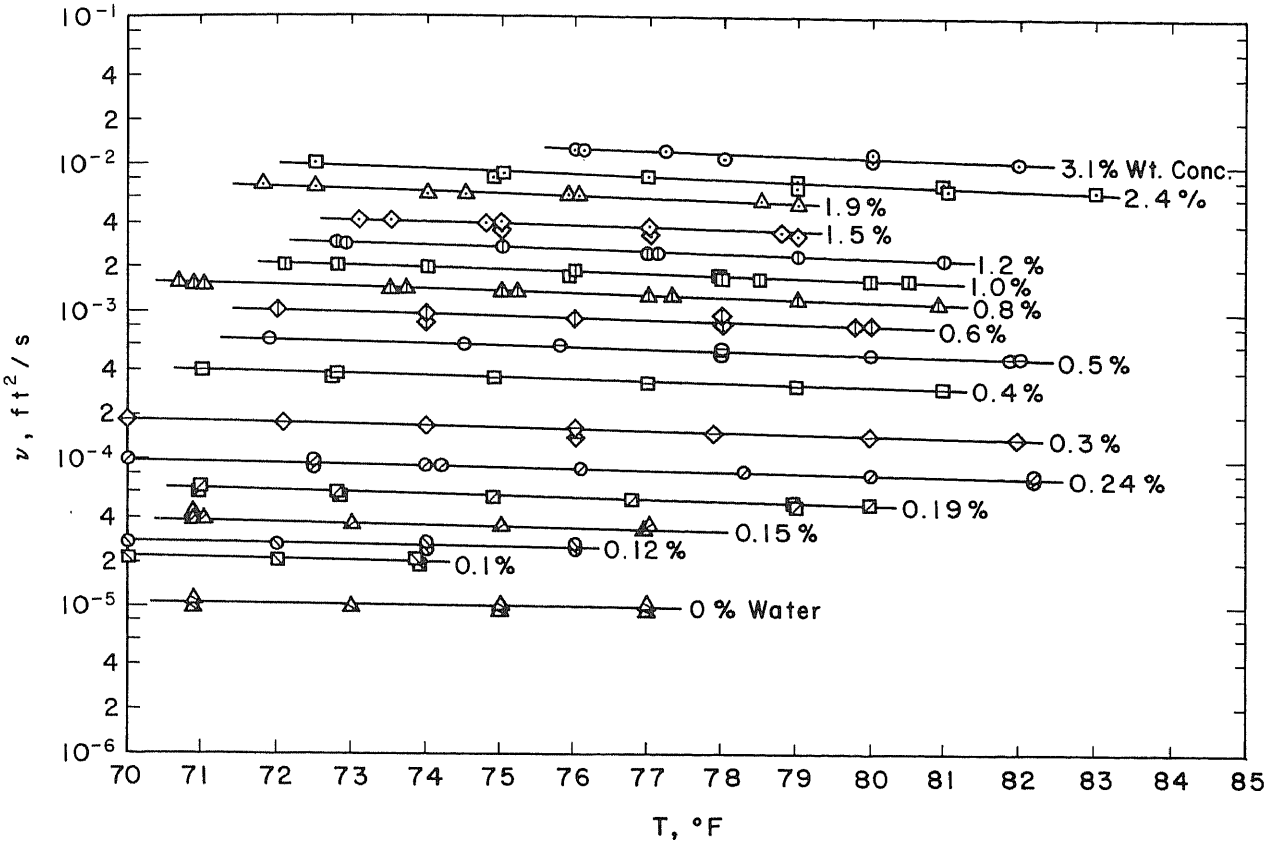

FIGURE 4.—Viscosities of working fluids for solutions of various nominal concentrations.

shift caused by boundary roughness, and the function $(\Pi/\kappa)[\omega(y/\delta)]$ is Coles' wake function (*4*), in which Π is the coefficient of wake strength. The function $f(U_* y/\nu)$ is the "standard" velocity-profile function that can be derived from simple dimensional analysis or from mixing-length theory (*3*).

Velocity profiles were measured in the model facility with an appropriately designed and calibrated total-head tube (*2*) and a differential pressure transducer. The total-head tube was inserted through the packing gland (fig. 1, m). It was constructed so that its tip would traverse a vertical located 3.2 ft from the leading edge of the test bed, or just ahead of the transducer insertion port (fig. 1, k). In making the velocity measurements, we took the virtual origin of the profile as one-fifth of a sphere diameter ($0.2D$ or $D/5$) below the top plane of the bed, as recommended by Einstein and El-Samni (*5*).

The velocity profiles were plotted in U/U_m $(U_m y/\nu)$ coordinates, and U_* and $\Delta U/U_*$ were estimated, using an adaptation of the cross-plot method (*3*).

In figure 6, the velocity shift $\Delta U/U_*$ is plotted

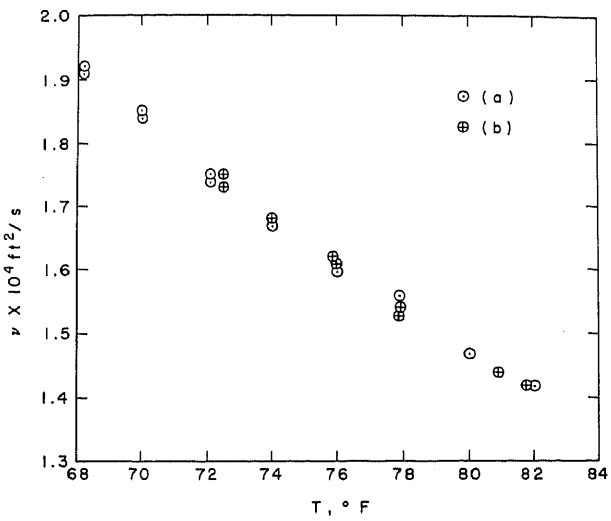

FIGURE 5.—Viscosity-temperature curve for a 0.3% polymer solution (a) after initial mixing, (b) after 7 hours of pumping during experiments.

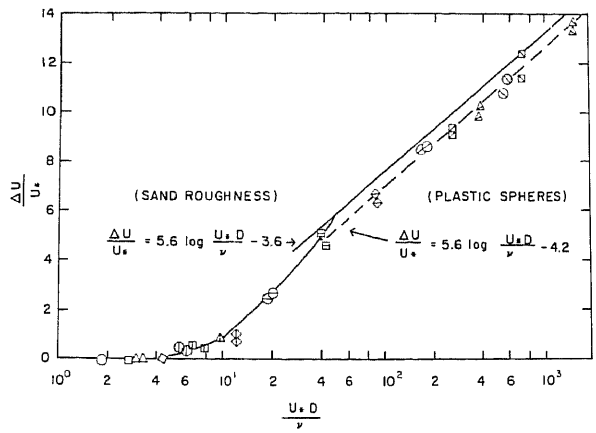

FIGURE 6.—Velocity-shift function.

against the bed-shear Reynolds number:

$$\mathbf{R}_*=\frac{U_*D}{\nu}. \tag{5}$$

Figure 6 shows that bed roughness begins to affect the flow at U_*D/ν equal to approximately 4. The transition regime ends, and the fully rough flow begins at about 50. In the fully rough regime, the function is

$$\frac{\Delta U}{U_*}=5.6\log\left(\frac{U_*D}{\nu}\right)-4.2, \tag{6}$$

which is identical to that for sand roughness, except the constant is 4.2 rather than 3.6, indicating that a bed of closely packed spheres is slightly smoother than a bed of natural sand particles. The above results agree generally with those of other experimenters (*10*).

The velocity profiles are plotted in figure 7. The functions included in the figure are, except for the introduction of $\Delta U/U_*$, the usual

$$\frac{U}{U_*}=\frac{U_*y}{\nu} \tag{7}$$

for the viscous sublayer, and the Karman-Prandtl law of the wall,

$$\frac{U}{U_*}=\frac{2.303}{\kappa}\log\left(\frac{U_*y}{\nu}\right)+4.9, \tag{8}$$

for the inertial region. For plotting figure 7, the Karman constant, κ, in equation 8 was taken as 0.41. The dash curve in the figure is the usual empirical transition function between the viscous and inertial regions. The velocity

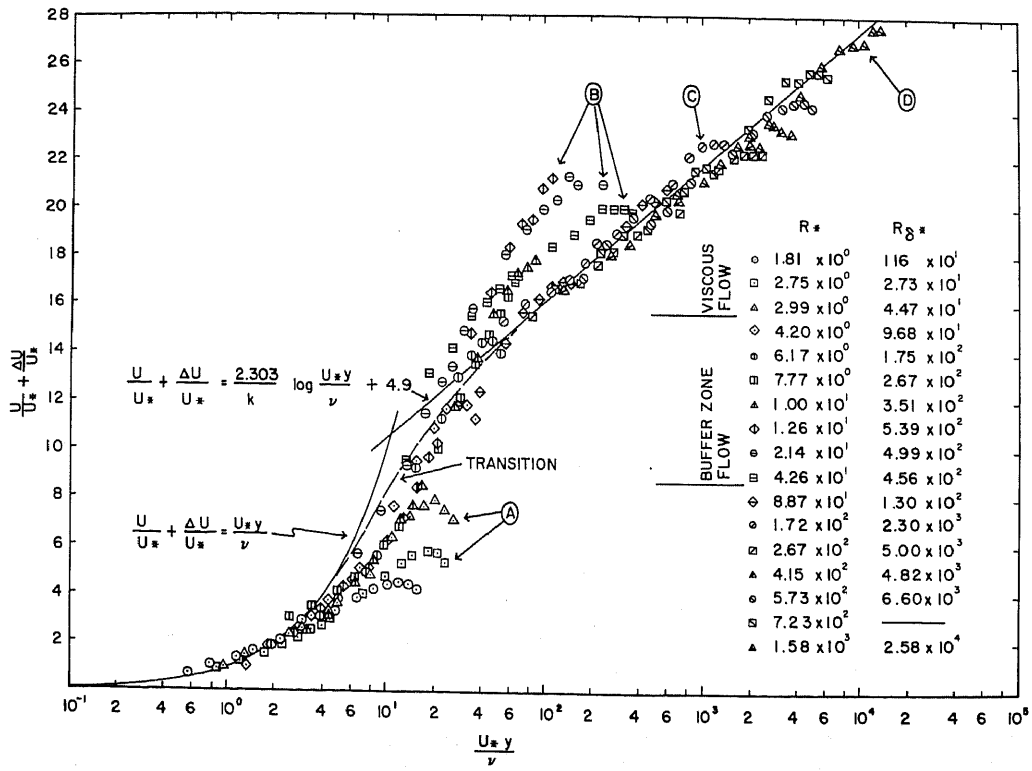

FIGURE 7.—Typical velocity profiles.

profiles labeled A in the figure are characteristic of totally viscous flow and have the equation

$$\frac{U}{U_m} = \frac{y}{\delta}\left(2 - \frac{y}{\delta}\right), \tag{9}$$

which is expanded to

$$\frac{U}{U_*} = \left(\frac{U_* y}{\nu}\right)\left(\frac{U_m}{U_*}\right)\left(\frac{\nu}{U_* \delta}\right)\left(2 - \frac{y}{\delta}\right), \tag{10}$$

for plotting in figure 7. These profiles are asymptotic to the viscous-sublayer function. The profiles labeled B are typical of flows where the displacement Reynolds number,

$$\mathbf{R}_{\delta^*} = \left(\frac{U_m}{\nu}\right)\int_0^{\delta}\left(1 - \frac{U}{U_m}\right) dy, \tag{11}$$

is less than 725 (*8*). These flows have a strong wake component and no logarithmic region. Profiles labeled C are typical of flows with $\mathbf{R}_{\delta^*}$ greater than 725, with significant intensity of turbulence in the inner part of the conduit. These profiles show both a logarithmic part and a wake region. As conduit turbulence increases, the wake component decreases (*4*), and profiles like D appear. These profiles have a logarithmic region but no wake region.

The bed-shear Reynolds number ($\mathbf{R}_*$) is the independent variable on which the velocity reduction in figure 6 depends. This Reynolds number is an indicator as to whether the flow over the bed is hydraulically smooth or rough, and whether or not a particle on the bed is experiencing viscous or turbulent approach flow. Thus, $\mathbf{R}_*$ is one type of particle Reynolds number, a second is the conventional form

$$\mathbf{R}_e = \frac{U_0 D}{\nu}, \tag{12}$$

where U_0 is the approach-flow-velocity vector acting along a line through the particle center. This Reynolds number characterizes the local flow around an isolated streambed particle and serves as the primary independent similitude parameter in lift and drag coefficient studies.

The joint variation of $\mathbf{R}_*$ and $\mathbf{R}_e$ is plotted in figure 8. Also included for comparison are the ranges of $\mathbf{R}_e$ obtained by Coleman (*3*) and Aksoy (*1*), and the ranges of $\mathbf{R}_*$ obtained by Watters and Rao (*9*). Apparently, the facility described here has broader experimental potential than those used in the other model studies. The capability of operating over a range from totally viscous flows to fully turbulent rough boundary flows is particularly

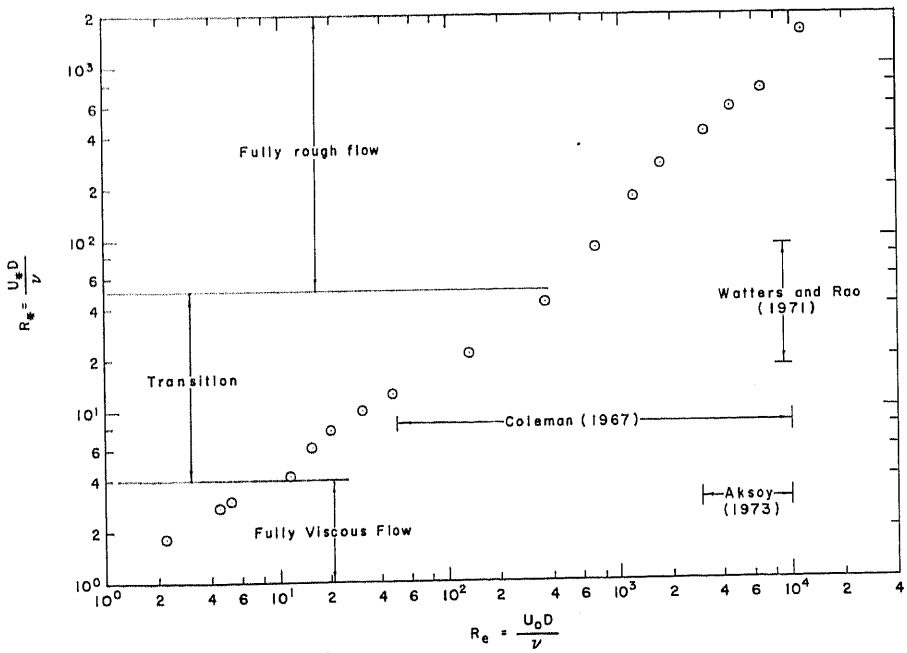

FIGURE 8.—Range of conditions attainable in the model facility.

advantageous for streambed-particle model studies.

CONCLUSIONS

By using a water-tunnel facility and HEC solutions with a wide range of viscosities as working fluids, researchers can conduct streambed-particle model studies over a wider range of Reynolds numbers than obtained previously. Particle Reynolds numbers from 1.0 to 10,000 can easily be obtained, and flow conditions can range from completely viscous to completely hydraulically rough.

LITERATURE CITED

(1) Aksoy, S. 1973. Fluid force acting on a sphere near a solid boundary. Proc. 15th Congr. Int. Assoc. Hydraul. Res. 1: 217–224.

(2) Bryer, D. W., and Pankhurst, R. C. 1971. Pressure probe methods for determining wind speed and flow direction. 125 pp. H.M. Stationery Office, London.

(3) Coleman, N. L. 1967. A theoretical and experimental study of drag and lift forces acting on a sphere resting on a hypothetical streambed. Proc. 12th Congr. Int. Assoc. Hydraul. Res. 3: 185–192.

(4) Coles, D. 1956. The law of the wake in the turbulent boundary layer. J. Fluid Mech. 1: 191–226.

(5) Einstein, H. A., and El-Samni, E. A. 1949. Hydrodynamic forces on a rough wall. Rev. Mod. Phys. 21(3): 520–524.

(6) Huang, T. T., and Santelli, N. 1971. Drag reduction and degradation of dilute polymer solutions in turbulent pipe flows. Nav. Ship Res. Dev. Cent. (Washington, D.C.) Rep. 3677, 33 pp.

(7) Scottron, V. A. 1967. Turbulent boundary layer characteristics over a rough surface in an adverse pressure gradient. Nav. Ship Res. Dev. Cent. (Washington, D.C.) Rep. 2659, 154 pp.

(8) Schubauer, G. B., and Tchen, C. M. 1961. Turbulent flow. 123 pp. Princeton University Press, Princeton.

(9) Watters, G. Z., and Rao, M. V. 1971. Hydrodynamic effects of seepage on bed particles. J. Hydraul. Div., Proc. Am. Soc. Civ. Eng., 97 (HY3): 121–439.

(10) White, F. M. 1974. Viscous fluid flow. 725 pp. McGraw-Hill, New York.

*1976 G.P.O. 1750-S/671-583/91